NASA TECHNICAL MEMORANDUM

NASA TM X-71633

NASA TM X-71633

PREDICTION OF COMPRESSOR STALL FOR DISTORTED AND UNDISTORTED FLOW BY USE OF A MULTISTAGE COMPRESSOR SIMULATION ON THE DIGITAL COMPUTER

by Carl J. Daniele and Fred Teren
Lewis Research Center
Cleveland, Ohio 44135

TECHNICAL PAPER to be presented at
Thirteenth Aerospace Sciences Meeting sponsored
by American Institute of Aeronautics and Astronautics
Pasadena, California, January 20-22, 1975

PREDICTION OF COMPRESSOR STALL FOR DISTORTED AND UNDISTORTED FLOW BY USE OF A MULTISTAGE COMPRESSOR SIMULATION ON THE DIGITAL COMPUTER

Carl J. Daniele and Fred Teren
National Aeronautics and Space Administration
Lewis Research Center
Cleveland, Ohio

E-8171

Abstract

A simulation technique is presented for the prediction of compressor stall for axial-flow compressors for clean and distorted inlet flow. The simulation is implemented on the digital computer and uses stage stacking and lumped-volume gas dynamics. The resulting nonlinear differential equations are linearized about a steady-state operating point, and a Routh-Hurwitz stability test is performed on the linear system matrix. Parallel compressor theory is utilized to extend the technique to the distorted inlet flow problem. The method is applied to the eight-stage J85-13 compressor. Analytical stall prediction for the undistorted stall line shows good agreement with experimental results. The predicted stall line for distorted inlet flow is in agreement with experimental results only for large distortion extents and/or low distortion levels. Results for low distortion extents and high distortion level do not agree with experimental results.

Nomenclature

$\mathcal{A}$	area, m^2; ft^2
C	coefficient, rpm^2/K^2; $rpm^2/{}^oR^2$
CONST	constant for weight flow derivatives, N/m^2; lbf/ft^2
g	gravitational constant, $1.0(kg\text{-}m)/(N\text{-}sec^2)$; $32.17(lbm\text{-}ft)/(lbf\text{-}sec^2)$
K	coefficient, rpm-sec/m; rpm-sec/ft
KCHOK	choked flow coefficient, $(kg\text{-}\sqrt{K})/(N\text{-}sec)$; $(lbm\text{-}\sqrt{{}^oR})/(lbf\text{-}sec)$
L	length, m; ft
N	rotational speed, rpm
P	pressure, N/m^2; lbf/ft^2
P2	input pressure, N/m^2; lbf/ft^2
R	universal gas constant, $287(N\text{-}m)/(kg\text{-}K)$; $53.3(lbf\text{-}ft)/(lbm\text{-}{}^oR)$
T	temperature, K; ^oR
T2	input temperature, K; ^oR
t	time, sec
V	volume, m^3; ft^3
v	velocity, m/sec; ft/sec
$\dot{W}$	weight flow, kg/sec; lbm/sec
γ	ratio of specific heats
δ	ratio of total pressure to sea level pressure
θ	ratio of total temperature to sea level temperature
ρ	weight density, kg/m^3; lbm/ft^3
Φ	flow coefficient
ψ^P	pressure coefficient
ψ^T	temperature coefficient

Subscripts:

b	variable associated with stage bleed
c	variable associated with stage characteristic
h	variable associated with undistorted side of compressor
ℓ	variable associated with distorted side of compressor
n	stage number designation
OGV	outlet guide vanes
s	static condition
t	total condition
v	variable associated with stage volume
z	axial direction
1,2,...,8	stage numbers
9	burner volume
10	nozzle exit

Superscripts:

$\dot{}$	derivative with respect to time
$\bar{}$	maximum value of quantity used for normalizing

I. Introduction

The transient performance of airplane propulsion systems using axial-flow compressors is greatly affected by the compressor stall characteristics. Compressor stall adversely affects engine performance by reducing thrust and engine airflow, and can cause inlet unstarts in supersonic aircraft. The stall characteristics of axial-flow compressors are directly affected by inlet distortion. Thus, the need for determining the stall line for these compressors under both distorted and undistorted inlet flow conditions is evident.

Experimental methods are generally used to determine stall lines for axial-flow compressors. However, engine experiments to define stall lines are costly and time consuming; thus, mathematical techniques to predict compressor stall conditions are being sought and developed. The procedures in use at present are one-dimensional and require well defined stage pressure and temperature characteristics. These characteristics must be determined experimentally. One method used to predict compressor stall is presented in reference 1, in which the undistorted stall line for the J85-13 axial-flow compressor was determined from an analog simulation and compared to experimental results. Recently, this work has been extended to digital computers.[2] Both simulations employ compressor stage stacking and lumped volume gas dynamics. On the analog computer, a limit cycle or instability of the time varying solution is correlated with experimentally observed compressor stall. The digital method involves linearization of the nonlinear system of equations (state equations) which defines the compressor simulation about a steady-state operating point, thereby obtaining a linear system matrix. System stability at this compressor operating point is then determined by a Routh-Hurwitz test of the system matrix, using digital routines found in reference 3. In reference 2, the stall line for the J85-13 was determined by the digital stability analysis. Comparison with the stall line generated by the analog simulation from reference 1 showed good agreement.

A technique which is sometimes useful in predicting stall for distorted inlet flow is parallel compressor theory (first postulated in ref. 4). The theory assumes that a compressor with distorted inlet flow can be represented by two fictional compressors, one having an inlet pressure equal to the distorted or low total pressure, and the other having an inlet total pressure equal to the undistorted or high total pressure. The distortion at the inlet is assumed to have a square wave form. Both compressors are assumed to discharge to a common static pressure and operate on the previously determined clean inlet speed line. No circumferential flow is exchanged between the two compressors. Stall is assumed to occur when the pressure ratio of the "low compressor" is equal to the clean inlet stall pressure ratio. Prior knowledge of an experimentally determined clean inlet stall pressure ratio is therefore necessary.

This theory has been investigated in references 5 through 8. In these references it is observed that parallel compressor theory gives accurate stall prediction for large distortion extent, but becomes progressively more conservative as extent decreases.

In this paper a method is described for predicting stall line location for circumferentially distorted inlet flow conditions which combines the digital stability analysis of reference 2 with a parallel compressor model. The objectives of this analysis are to eliminate the need for a knowledge of a reference clean inlet stall pressure ratio and to improve the accuracy of stall line prediction. The digital simulation as in reference 2, used stage stacking and lumped volume gas dynamics. Two separate compressors were simulated with a static pressure balance in the burner volume at steady-state. The combined nonlinear system of equations is linearized and checked for stability as in reference 2. With this model, the predicted compressor stall point depends on the operating point of the undistorted side as well as the distorted side.

Results are presented first which compare the analytically predicted stall line with experimental data for undistorted flow. Then using a parallel compressor model and the digital stability analysis, stall points are predicted for varying distortion extents and intensities and are compared with experimental results.

II. Engine Description

The analysis in this report is applied to the J85-13 afterburning turbojet engine. The engine consists of an eight-stage, axial-flow compressor, a two-stage turbine, variable inlet and outlet guide vanes, controlled interstage bleeds, and variable exhaust nozzle. The inlet guide vanes are scheduled as a function of corrected speed; the outlet guide vanes are fixed, but the pressure drop across them varies with corrected weight flow. The interstage bleeds are on the third, fourth, and fifth compressor stages and are also scheduled as a function of corrected speed. (The bleeds are closed above 94.0 percent corrected speed, are full open at 80 percent speed and below, and vary with speed in between.)

III. Simulation Model: Undistorted Flow

The single compressor with undistorted inlet flow is modeled as follows. The multistage compressor portion of the simulation uses steady-state stage characteristics and an associated stage volume for gas dynamics to represent individual stages. Each compressor stage is modeled with pressure and temperature maps; each volume, with lumped continuity, energy, and momentum equations. The inlet and outlet guide vanes are modeled as pressure drops into and out of the first and last stages, respectively, the amount of pressure drop being a function of corrected speed. Bleed flows are included for the third, fourth, and fifth stages; the amount of bleed flow is also a function of corrected speed. The bleeds are assumed choked. Between the last compressor stage and turbine, a burner volume is modeled. No heat addition is included, however, because only the compressor, rather than the whole engine, is of interest for this report. Behind the burner a choked nozzle is used to terminate the simulation. The choked nozzle simulates a choked turbine in the actual engine. A schematic of an ideal compressor stage is shown in figure 1.

Steady-State Equations

The steady-state performance of the axial-flow compressor is calculated by using the stage stacking technique described in reference 1. In this technique the discharge conditions of one stage are used as the inlet conditions to the next stage. The steady-state performance for each stage is given by pressure and temperature rise coefficients ψ_c^P and ψ_c^T. These coefficients are defined as

$$\psi_{c,n}^{P} = \frac{C_n T_{tv,n-1}}{N^2}\left[\left(\frac{P_{tc,n}}{P_{tv,n-1}}\right)^{2/7} - 1\right] \qquad (1)$$

$$\psi^T_{c,n} = \frac{C_n}{N^2}\,(T_{tc,n} - T_{tv,n-1}) \qquad (2)$$

Representative maps of ψ^P and ψ^T as a function of flow coefficient Φ are shown in figure 2. The flow coefficient is defined as

$$\Phi_{c,n} = \frac{K_n}{N}\,v_{zc,n} \qquad (3)$$

The steady-state performance of the burner volume is modeled by assuming that the pressure, temperature, and weight flow into and out of the volume are the same. The nozzle and bleed ports are assumed choked, with the amount of bleed flow area a function of corrected speed. The choked flow equation used is

$$\dot{W} = \text{KCHOK}\,\mathscr{A}\,\frac{P_t}{\sqrt{T_t}} \qquad (4)$$

The steady-state equations are used to determine an operating point on a speed line.

Dynamic Equations

Compressor dynamics are simulated by using a lumped volume for each stage. Each lumped volume is located just downstream of the stage's active element. The volume dynamics are modeled through the application of continuity, energy, and momentum equations. The equations are

$$\frac{d}{dt}\,(\rho_{sv,n}) = \frac{1}{V_n}\,(\dot{W}_{c,n} - \dot{W}_{c,n+1}) \qquad (5)$$

$$\frac{d}{dt}\,(\rho_{sv,n}T_{tv,n})$$

$$= \frac{\gamma}{V_n}\,[T_{tc,n}\dot{W}_{c,n} - T_{tv,n}(\dot{W}_{c,n+1} + \dot{W}_{b,n})] \qquad (6)$$

and

$$\frac{d}{dt}\,(\dot{W}_{c,n}) = \frac{\mathscr{A}_n g}{L_n}\,(P_{tc,n} - P_{tv,n}) \qquad (7)$$

While the equation of state for the gas in the volume is

$$P_{tv,n} = R\rho_{sv,n}T_{tv,n} \qquad (8)$$

No dynamic effects are modeled for the inlet and outlet guide vanes, interstage bleeds, or choked nozzle. A lumped volume is included in the burner.

The dynamic equations used to model the burner volume are

$$\frac{d}{dt}\,(\rho_{sv,9}T_{tv,9}) = \frac{\gamma T_{tv,9}}{V_9}\,[\dot{W}_{c,9} - \dot{W}_{c,10}] \qquad (9)$$

where $\dot{W}_{c,10}$ is the choked nozzle flow, and

$$\frac{d}{dt}\,(\dot{W}_{c,9}) = \frac{\mathscr{A}_9 g}{L_9}\,(P_{tc,9} - P_{tv,9}) \qquad (10)$$

with the temperature in the burner volume assumed equal to the temperature in the outlet guide vanes:

$$T_{tv,9} = T_{tc,9} = T_{tv,8} \qquad (11)$$

Thus, the undistorted compressor simulation consists of 26 state equations - three for each of the eight compressor stages and two for the burner volume.

IV. Simulation Model: Distorted Flow

Parallel compressor theory is used as a basis for extending the undistorted inlet flow model to distorted inlet flow conditions. A schematic diagram of the parallel compressor model is shown in figure 3. The assumptions made are that two separate compressors are modeled with different total pressures at their inlet and that no crossflow occurs between the compressor segments. At steady state, static pressure is balanced at the discharge of the compressor segments.

Steady-State Equations

Two completely separate compressors are modeled with different total pressures at their inlets. The steady-state performance of each compressor is calculated using equations (1) to (3) for the eight compressor stages and the stage maps determined from clean inlet flow experimental tests.

However, additional equations are added in the burner volume to account for the different exit conditions for each compressor segment. In the burner volume, the weight flows from the two compressors are added and the exit temperatures are mass averaged, thus

$$\dot{W}_{c,9} = \dot{W}_{c,9\ell} + \dot{W}_{c,9h} \qquad (12)$$

$$T_{tv,9} = \frac{(\dot{W}_{c,9\ell}T_{tv,9\ell} + \dot{W}_{c,9h}T_{tv,9h})}{\dot{W}_{c,9\ell} + \dot{W}_{c,9h}} \qquad (13)$$

The total pressure in the burner volume is calculated by using the static pressure and the compressible flow equations. Once the pressure, temperature, and weight flow are calculated, a choked nozzle equation (4) is used to terminate the model.

Dynamic Equations

For both compressors simulated, the dynamic equations for the single compressor (eqs. (5) to (8)) apply for the eight compressor stages. In these equations, however, the volumes and areas are sized to account for the distortion extent. Equations (9) and (10) used to simulate dynamics in the burner volume are modified to account for the parallel compressors by

$$\frac{d}{dt}\,(\rho_{sv,9}T_{tv,9}) = \frac{\gamma}{V_9}\,T_{tv,9}(\dot{W}_{c,9\ell} + \dot{W}_{c,9h} - \dot{W}_{10}) \qquad (14)$$

where $\dot{W}_{10}$ is the choked nozzle flow. Also

$$\frac{d}{dt}\,(\dot{W}_{c,9h}) = \frac{\mathscr{A}_{9,h} g}{L_9}\,(P_{tc,9h} - P_{tv,9} - \text{CONST}_h) \qquad (15)$$

and

$$\frac{d}{dt}\left(\dot{W}_{c,9\ell}\right) = \frac{\mathscr{A}_{9,\ell}g}{L_9}\left(P_{tc,9\ell} - P_{tv,9} - CONST_\ell\right) \quad (16)$$

where CONST is a steady-state pressure drop and is set such that $d/dt\ W_{c,9}$ is equal to zero in steady state. The temperature in the burner volume is calculated from equation (13). Thus, the parallel compressor model consists of 51 state equations - twenty four for each compressor segment and three for the burner volume.

V. Stability Analysis

The most direct way to determine the stability of a system of nonlinear differential equations is to obtain the transient response to a small disturbance, starting at a steady-state operating point. A stable system will return to the steady-state condition once the disturbance has subsided. An unstable system, however, will either diverge or undergo limit cycle oscillations. This method of stall prediction was used in reference 1 wherein an analog computer simulation was used to obtain the transient solution and predict compressor stall for clean inlet flow for the J85 engine.

It was desired to extend the stability analysis technique of reference 1 to the prediction of compressor stall for distorted inlet flow. This requires the simulation of two separate compressors, as discussed earlier. It was not possible to construct such a simulation on the analog computers at the Lewis Research Center, because the large amount of equipment required exceeded the amount of available analog equipment. Therefore, it was decided to construct an equivalent simulation on the digital computer. Results from this simulation (unpublished) showed that a time step of 50 microseconds or less was required to avoid numerically induced instability. As a result, about one hour of computer time was required for 1 second of real-time data. Because of this, the computer time required to conduct substantial stability analysis on the digital computer was prohibitive.

In order to make use of the digital computer for stability prediction and avoid large computer times, a new stability analysis technique was developed and is the subject of reference 2. This technique does not require numerical integration of differential equations. In addition to stability prediction, the method is very useful and efficient for the calculation of frequency responses, eigenvalues, and eigenvectors, as shown in reference 2.

The stability analysis in reference 2 is applied to the model by first determining a steady-state point on a speed line. The nonlinear system of equations (state equations) which defines the compressor simulation about the operating point is linearized and a linear system matrix is obtained. The elements of the system matrix are the partial derivatives of the state equations with respect to the state variables. The linearization of the state equations and calculation of the matrix elements are accomplished by finite differences on the digital computer. The stability of the system matrix is checked by a Routh-Hurwitz test. When this test indicates instability, the linear system is unstable and the nonlinear system is also unstable through application of the first method of Lyapunov.[9]

The stability analysis is first applied to the undistorted single compressor model. A point is chosen on a speed line and its stability determined by the Routh-Hurwitz test. If it is stable, points are chosen at successively lower flow rates on the speed line until instability is indicated. The stability analysis is also applied to the prediction of stall for distorted inlet flow by using the 51-variable dynamic model described earlier. This method should improve on classical parallel compressor theory since it does not require an experimentally determined clean inlet stall point as reference. Also there should be an improvement in overall stall prediction since the whole compressor model (both undistorted and distorted segments) is considered in determining compressor stability.

V. Results

Results are presented first which compare the analytically predicted stall line with experimental data for undistorted flow. Then using a parallel compressor model and the digital stability analysis, stall points are predicted for varying distortion extents and intensities and compared with experimental results.

Data Base

The experimental data used is from a recent test of a J85 engine in a Lewis altitude facility where stall line definition for both undistorted and distorted inlet flow was accomplished. Stage temperature and pressure maps were determined and used in the simulation. These stage maps give a mean line representation of the stage characteristics - data is taken at the stator exit at three radial positions and those results are area weighted radially to get mean line values. From these values one set of pressure and temperature stage maps is determined. This set of maps is used for all compressor speeds.

Undistorted Stall Line

The overall compressor map as determined by the simulation is compared to experimental results in figure 4. This figure shows overall compressor ratio as a function of weight flow corrected to the compressor face. Speeds of 80, 87, 94, and 100 percent are shown. The circles represent experimental data points and the solid lines are the analytical speed lines. Darkened triangles and circles represent the analytical and experimental stall points, respectively. The dashed line is the experimental stall line. Stall points predicted by the stability analysis agree well with experimental results. The analytical speed lines agree well with the experimental speed lines except at 94 percent. However, this speed line differs from previous J85 experimental data and is suspect. The fact that the interstage bleeds begin to open at 94 percent speed may have some effect on the shape of the speed line and warrants further investigation. Therefore, in this report, further results for the 94 percent speed line will be included but not discussed.

Distortion Results

The experimental data base for the analysis

consisted of four different density screens and four different distortion extents. Table I lists the different combinations of screens and extents used. Figure 5 shows the ability of the analysis to predict performance and stall limits. Figure 5(a) is for the 180 degree extent and 5(b) for the 30 degree extent. In both cases the results shown are for the medium density screen. Good performance and stall prediction is shown for the 80 and 100 percent speed lines in figure 5(a). Stall prediction for the 87 percent speed line is fair but there is good agreement with the experimental speed line.

In figure 5(b) there is good agreement between analytical and experimental speed lines. However, stall prediction is conservative in all cases with the 100 percent speed line being more acceptable. The analytical speed lines have also been calculated beyond the stall points, but the results are not shown here. The analytical speed lines diverge from the experimental results for weight flows below the predicted stall point.

Figure 6 shows the effect of varying distortion extent with constant screen density. Only experimental and analytical stall points, and not speed lines, are shown. Open symbols are analytical results and darkened symbols are experimental results. Figures 6(a), (b), and (c) show results for the high, medium, and low density screens, respectively. Figure 6(a) shows good agreement for the 180 degree extent but the agreement deteriorates at 90 and 60 degrees. As the screen density decreases (figs. 6(b) and (c)) the agreement for the small extents becomes better. Also, from figure 6(a), experimental results indicate (neglecting scatter) that the stall limit increases as extent decreases for fixed screen density as expected. However, the analytical results indicate the opposite effect.

Figure 7 shows the same data as figure 6 but is plotted to show the effect of screen density as distortion extent is held constant. In this figure also, only the experimental and analytical stall points are shown. Figure 7(a) shows that for the 180 degree extent, there is good agreement between the analytical and experimental results. Figures 7(b) and (c) with 90 and 60 degree extents, respectively, show increasing degradations in stall prediction. In all cases, however, the expected trend of decreasing compressor performance with increasing distortion level is present in the analytical results and also in the experimental results.

VII. Concluding Remarks

Presented in this report is the application of the compressor stall prediction method from reference 2 to an axial-flow compressor recently tested in a Lewis altitude facility. The test involved stall line definition for the compressor with both undistorted and distorted inlet flows. The stall prediction correlates well with experimental results for clean inlet flow. The inclusion of the stability analysis with the parallel compressor model used to simulate distorted inlet flow, however, produces mixed results. The correlation of instability with experimental stall is acceptable at 180 degree extent with all distortion levels and at smaller extents for small distortion levels. The correlation is not good for extents less than 180 degrees for large distortion levels. This is the same disadvantage as noted in references 5, 6, and 7 for stall determination using pure parallel compressor theory. Thus, no improvement has been made in compressor stall prediction with the addition of the stability analysis to the parallel compressor model.

The failure of the method to accurately predict stall for distortion extents less than 180 degrees may be related to the lack of coupling of the distorted and undistorted sectors in the compressor section itself. That is, as the parallel compressor model is presently incorporated in the analysis, the undistorted and distorted sectors both contribute to the stall prediction method, but only through the burner volume. Since the burner volume is much larger than the stage volumes, its dynamic contribution relative to the whole system is small. Therefore, one obvious modification to the analysis would be to permit interaction between undistorted and distorted sectors at each stage through circumferential crossflows in the stage volumes. Thus, the ability of the undistorted sector to provide a stabilizing influence on the distorted sector would be enhanced. The authors are currently modifying the simulation described in this report to allow for circumferential crossflows.

References

1. Willoh, R. G. and Seldner, K., "Multistage Compressor Simulation Applied to the Prediction of Axial Flow Instabilities," TM X-1880, 1969, NASA.

2. Daniele, C. J., Blaha, R. J. and Seldner, K., "Prediction of Axial Flow Instabilities in a Turbojet Engine by Use of a Multistate Compressor Simulation on the Digital Computer," TM X-3134, 1974, NASA.

3. Seidel, R. C., "Computer Programs for Calculation of Matrix Stability and Frequency Response from a State-Space System Description," TM X-71581, 1974, NASA.

4. Pearson, H., and McKenzie, A. B., "Wakes in Axial Compressors," Journal of the Royal Aeronautical Society, Vol. 63, No. 583, July 1959, pp. 415-416.

5. Korn, J. A., "Compressor Distortion Estimates Using Parallel Compressor Theory and Stall Delay," Journal of Aircraft, Vol. 11, No. 9, Sept. 1974, pp. 584-586.

6. Reid, C., "The Response of Axial Flow Compressors to Intake Flow Distortion," ASME Paper 69-GT-29, Cleveland, Ohio, Mar. 1969.

7. Melick, H. C., Jr. and Simpkin, W. E., "A Unified Theory of Inlet/Engine Compatibility," AIAA Paper 72-1115, New Orleans, La., Nov.-Dec. 1972.

8. Calogeras, J. E., Johnsen, R. L. and Burstadt, P. L., "Effect of Screen-Induced Total-Pressure Distortion on Axial-Flow Compressor Stability," TM X-3017, 1974, NASA.

9. Ogata, Katsuhiko, "State Space Analysis of Control Systems," Prentice-Hall, Inc., 1967.

Table I Combinations of screen densities and distortion extents

Screen density	$\% \frac{(P2_h - P2_\ell)}{P_{average}}$ * 80% speed	Distortion extent, deg			
		180	90	60	30
Low	2.083	X	X		
Medium	4.234	X	X	X	X
High	4.741	X	X	X	
Highest	7.163			X	

X denotes experimental data taken.

*The distortion levels given are indicative of the distortion levels for the screens. Slight differences in these numbers result at different speeds and along each speed line.

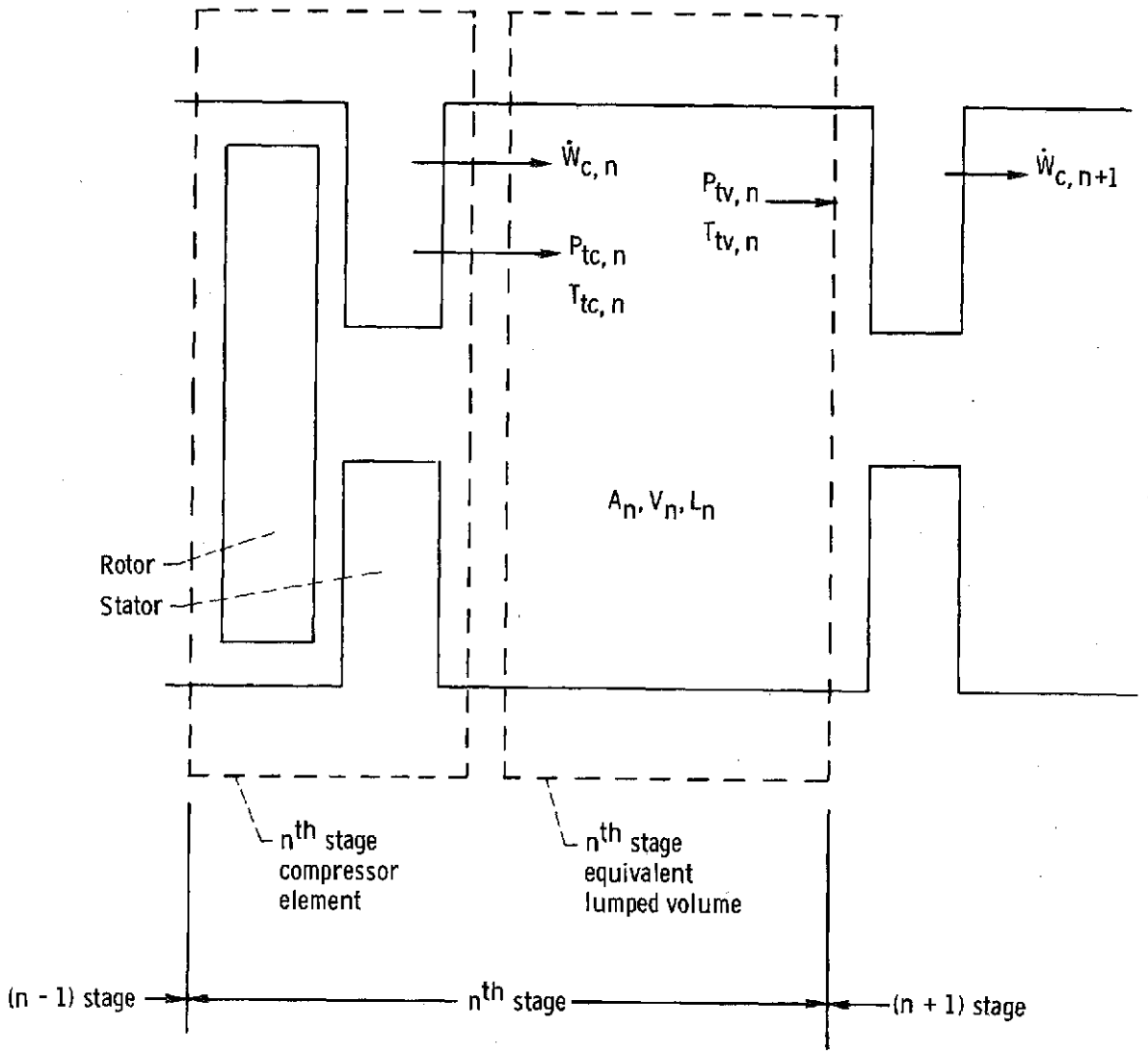

Figure 1. - Schematic of n^{th} stage compressor.

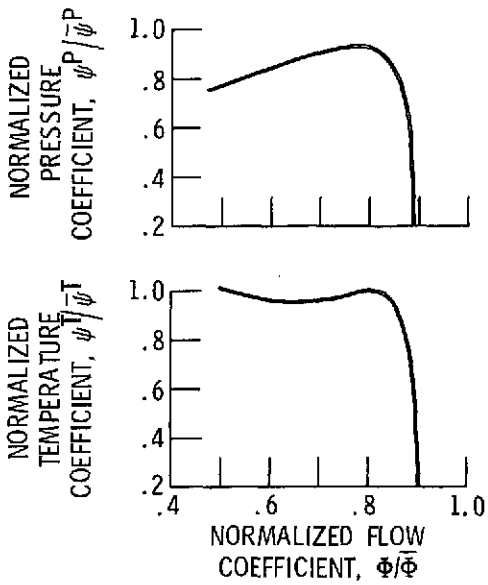

Figure 2. - Representative compressor stage pressure and temperature maps.

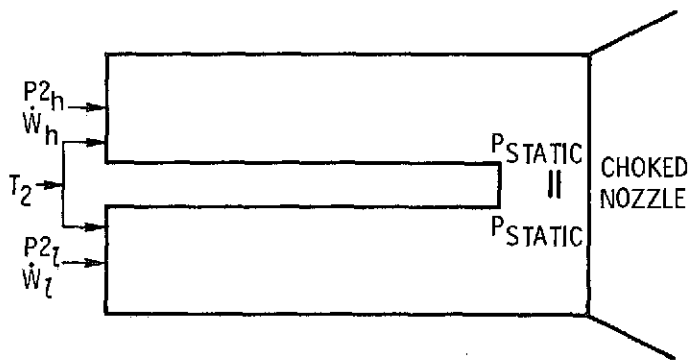

Figure 3. - Parallel compressor model.

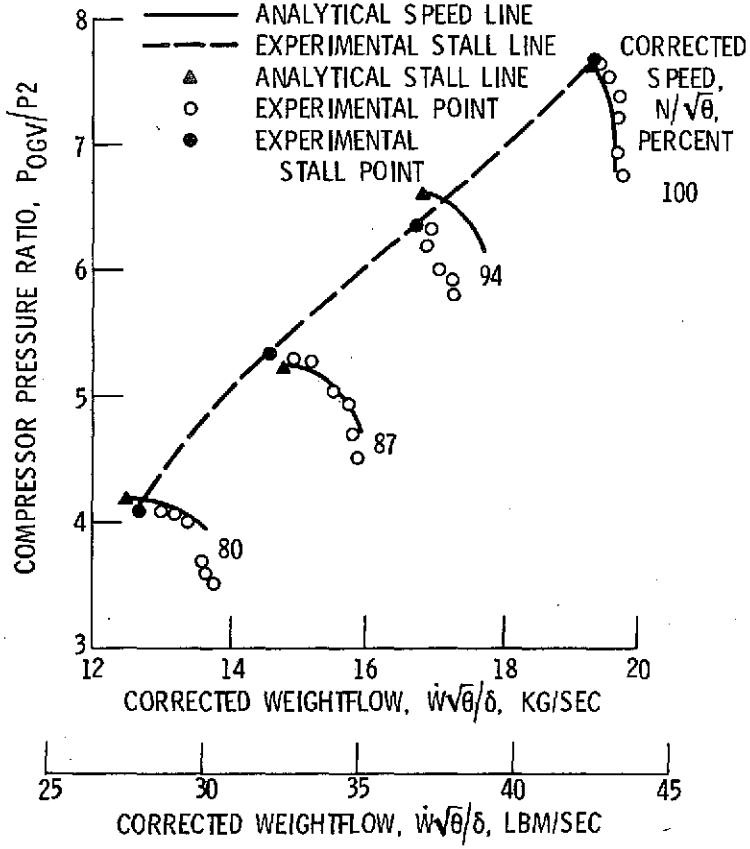

Figure 4. - Comparison of analytical and experimental stall lines. Undistorted flow.

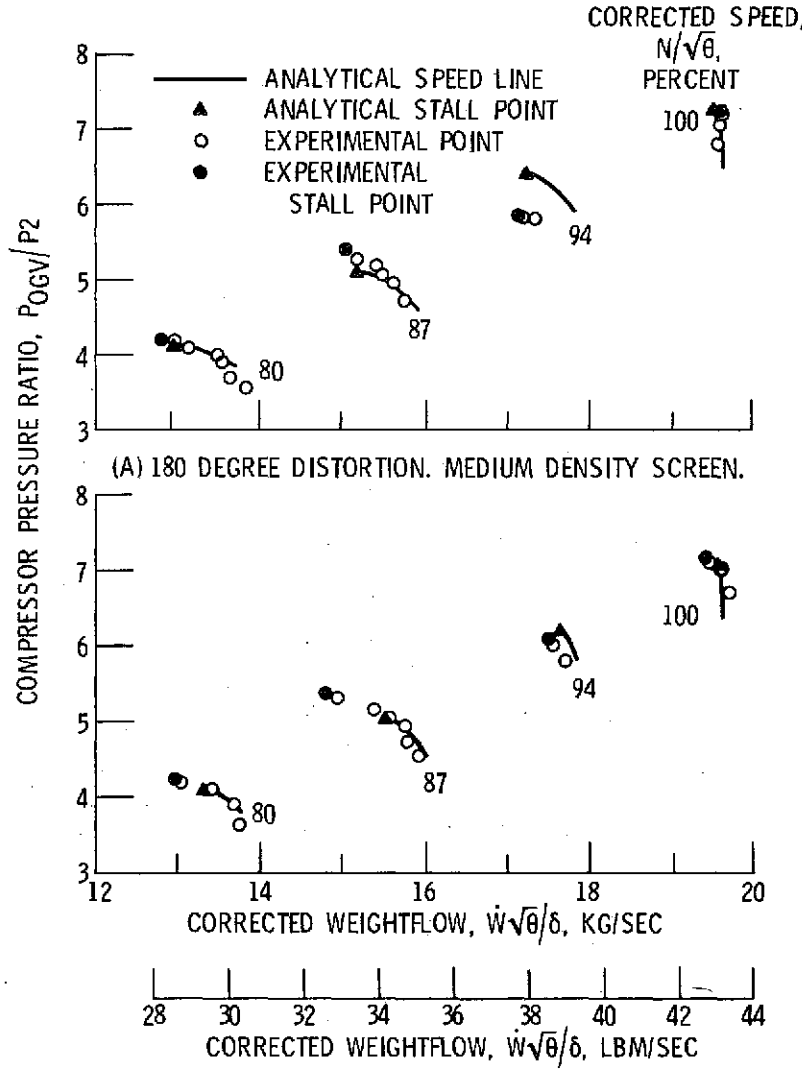

(A) 180 DEGREE DISTORTION. MEDIUM DENSITY SCREEN.

(B) 30 DEGREE DISTORTION. MEDIUM DENSITY SCREEN.

Figure 5. - Comparison of experimental and analytical results. Distorted inlet flow.

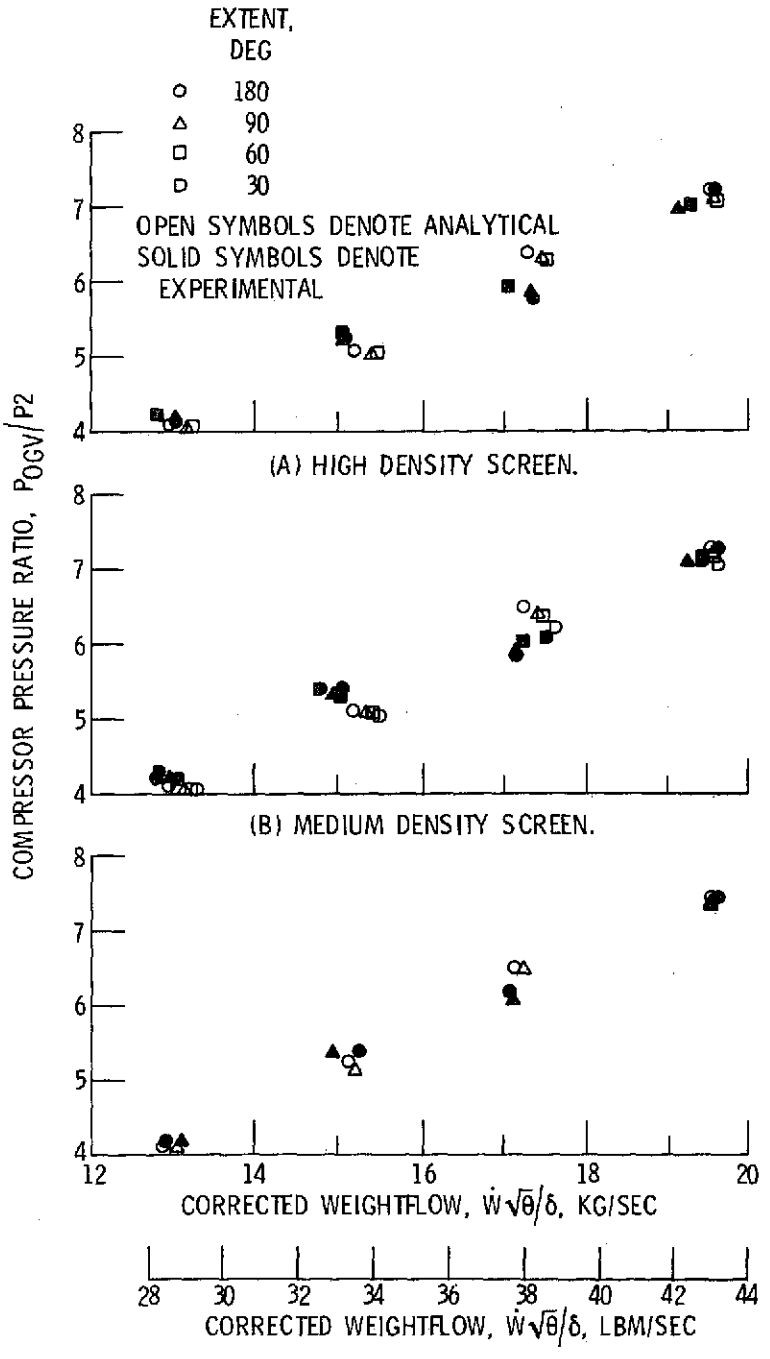

Figure 6. - Comparison of analytical and experimental stall points. Screen porosity constant.

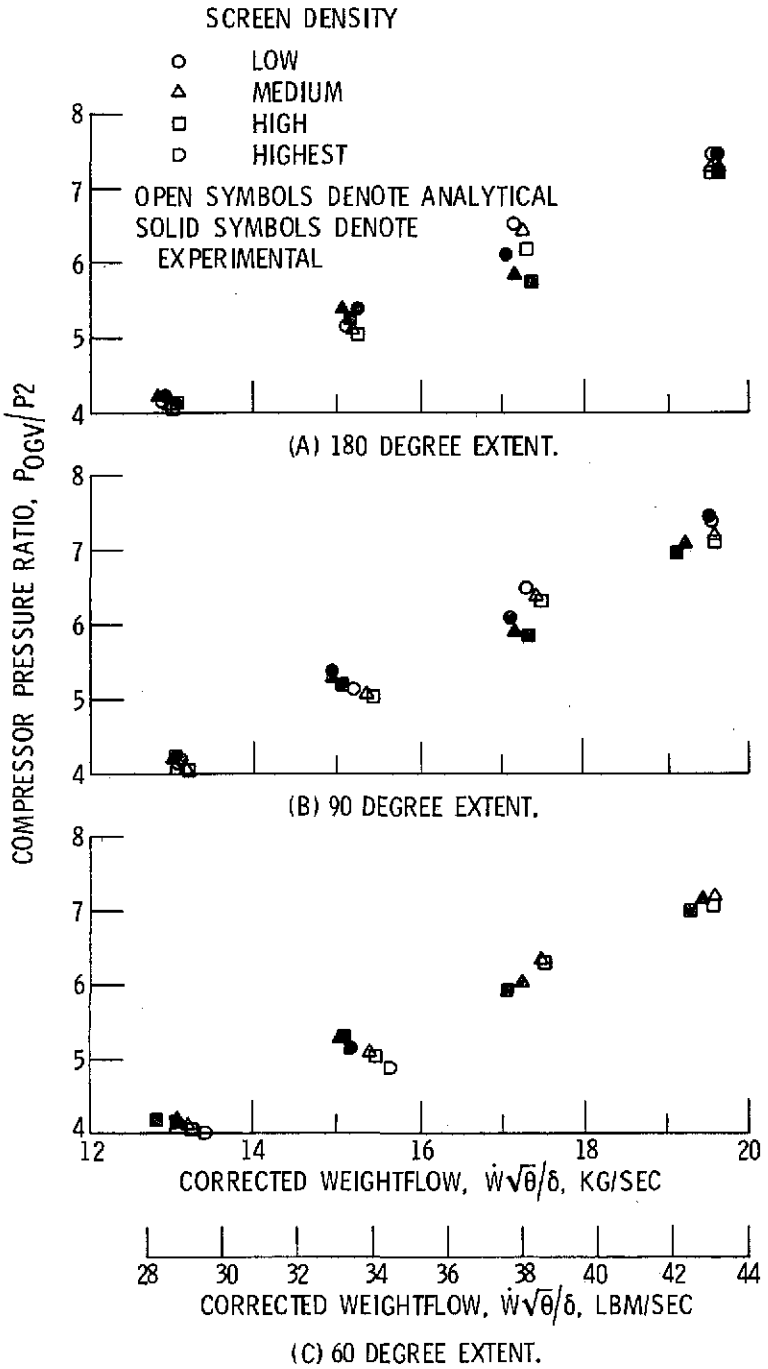

Figure 7. - Comparison of analytical and experimental stall points. Distortion extent constant.